JCI The Journal of Clinical Investigation

# *Mll* partial tandem duplication induces aberrant *Hox* expression in vivo via specific epigenetic alterations

Adrienne M. Dorrance, … , Guido Marcucci, Michael A. Caligiuri

*J Clin Invest.* 2006;116(10):2707-2716. https://doi.org/10.1172/JCI25546.

**Research Article** **Oncology**

We previously identified a rearrangement of *mixed-lineage leukemia* (*MLL*) gene (also known as *ALL-1, HRX*, and *HTRX1*), consisting of an in-frame partial tandem duplication (PTD) of exons 5 through 11 in the absence of a partner gene, occurring in approximately 4%–7% of patients with acute myeloid leukemia (AML) and normal cytogenetics, and associated with a poor prognosis. The mechanism by which the *MLL* PTD contributes to aberrant hematopoiesis and/or leukemia is unknown. To examine this, we generated a mouse knockin model in which exons 5 through 11 of the murine *Mll* gene were targeted to intron 4 of the endogenous *Mll* locus. $Mll^{PTD/WT}$ mice exhibit an alteration in the boundaries of normal *homeobox* (*Hox*) gene expression during embryogenesis, resulting in axial skeletal defects and increased numbers of hematopoietic progenitor cells. $Mll^{PTD/WT}$ mice overexpress *Hoxa7, Hoxa9*, and *Hoxa10* in spleen, BM, and blood. An increase in histone H3/H4 acetylation and histone H3 lysine 4 (Lys4) methylation within the *Hoxa7* and *Hoxa9* promoters provides an epigenetic mechanism by which this overexpression occurs in vivo and an etiologic role for *MLL* PTD gain of function in the genesis of AML.



# *Mll* partial tandem duplication induces aberrant *Hox* expression in vivo via specific epigenetic alterations

Adrienne M. Dorrance,[1,2] Shujun Liu,[1] Weifeng Yuan,[1] Brian Becknell,[1,3] Kristy J. Arnoczky,[3] Martin Guimond,[1] Matthew P. Strout,[1] Lan Feng,[1] Tatsuya Nakamura,[4] Li Yu,[1] Laura J. Rush,[2,5] Michael Weinstein,[6] Gustavo Leone,[4,5] Lizhao Wu,[4] Amy Ferketich,[5,7] Susan P. Whitman,[1,5] Guido Marcucci,[1,5] and Michael A. Caligiuri[1,2,3,4,5]

[1]Department of Internal Medicine, Division of Hematology and Oncology, [2]Department of Veterinary Biosciences, [3]Integrated Biomedical Science Graduate Program, [4]Department of Molecular Virology, Immunology and Medical Genetics, [5]Comprehensive Cancer Center, [6]Department of Molecular Genetics, and [7]Division of Biometrics, The Ohio State University, Columbus, Ohio, USA.

**We previously identified a rearrangement of *mixed-lineage leukemia* (*MLL*) gene (also known as *ALL-1, HRX*, and *HTRX1*), consisting of an in-frame partial tandem duplication (PTD) of exons 5 through 11 in the absence of a partner gene, occurring in approximately 4%–7% of patients with acute myeloid leukemia (AML) and normal cytogenetics, and associated with a poor prognosis. The mechanism by which the *MLL* PTD contributes to aberrant hematopoiesis and/or leukemia is unknown. To examine this, we generated a mouse knockin model in which exons 5 through 11 of the murine *Mll* gene were targeted to intron 4 of the endogenous *Mll* locus. $Mll^{PTD/WT}$ mice exhibit an alteration in the boundaries of normal *homeobox* (*Hox*) gene expression during embryogenesis, resulting in axial skeletal defects and increased numbers of hematopoietic progenitor cells. $Mll^{PTD/WT}$ mice overexpress *Hoxa7, Hoxa9*, and *Hoxa10* in spleen, BM, and blood. An increase in histone H3/H4 acetylation and histone H3 lysine 4 (Lys4) methylation within the *Hoxa7* and *Hoxa9* promoters provides an epigenetic mechanism by which this overexpression occurs in vivo and an etiologic role for *MLL* PTD gain of function in the genesis of AML.**

## Introduction

*Mixed-lineage leukemia* (*MLL*, also known as *ALL-1, HRX,* or *HTRX1*) is the human homolog of *Drosophila Trx* and is a maintenance factor for the homeobox (Hox) group of proteins, which play an important role in specifying cell fate during development and hematopoiesis (1). Approximately 4% of patients with de novo acute myeloid leukemia (AML) have balanced translocations or insertions that result in fusion of *MLL* at chromosome 11q23 with 1 of over 40 functionally divergent genes. Although a central mechanism responsible for malignant transformation as a result of these chromosomal translocations involving 11q23 is lacking, the N terminus of MLL, which contains the AT-hook DNA-binding motif and a region homologous to DNA methyltransferase, is always retained in the fusion protein while the C terminus, which contains the activation and SET domains, is always replaced by the fusion partner (2).

We discovered a rearrangement of *MLL* in AML patients whereby *MLL* is not fused with a partner gene but rather is consistently elongated with an in-frame partial tandem duplication (PTD) of exons 11-5 or 12-5 (former exon designations were 6-2 and 8-2) (3). In contrast with the myriad of *MLL* fusions in AML that result from chromosomal translocations, AML blasts with the MLL PTD retain the protein's C terminus, which contains the activation and SET domains and partially duplicates a region within the N terminus containing the AT-hook DNA-binding and repression domains (2). Approximately 4%–7% of AML patients with normal cytogenetics harbor the *MLL* PTD and carry an especially poor prognosis (4, 5).

*HoxA* genes are frequently overexpressed in leukemia (6). The mechanism by which the *MLL* PTD contributes to aberrant hematopoiesis and/or leukemogenesis is currently unknown, but given MLL's role as a maintenance factor for Hox proteins, 1 mechanism could involve deregulation of *Hox* gene expression. In in vitro model systems, WT MLL regulates certain *HOX* gene expression via epigenetic modification at *cis*-regulatory regions, i.e., histone H3/H4 acetylation and H3 lysine 4 (Lys4) methylation, the latter of which requires MLL's C terminus SET domain (7, 8). When the *MLL-AF9* fusion gene (the result of one of the most common MLL rearrangements) is transduced into $Mll^{-/-}$ cells, *Hoxa9* is overexpressed by an unknown mechanism that does not require binding of the MLL-AF9 fusion directly to the *Hoxa9* promoter (8). However, in another in vitro study, transduction of the MLL–*eleven nineteen leukemia* and the MLL–*FK506-binding protein* fusions into $Mll^{WT/WT}$ cells increased *Hoxa9* expression via H3 acetylation but without increased H3 Lys4 methylation (9). Likewise, when the *Mll-AF9* fusion was knocked in as an endogenous allele, mice showed *Hoxa9* overexpression and developed AML, but no epigenetic or other alteration could account for this overexpression (10, 11). This suggests distinct mechanisms for induction of *HOX* genes by WT MLL and fusions of MLL resulting from balanced chromosomal translocations.

Taspase 1 cleaves the approximately 430-kDa MLL protein into 2 smaller components, and this cleavage has been shown to

**Nonstandard abbreviations used:** AML, acute myeloid leukemia; BFU-E, burst-forming unit–erythroid; ChIP, chromatin IP; GEMM-CFU, granulocyte, erythroid, macrophage, megakaryocyte–CFU; Hox, homeobox; Lys4, lysine 4; MLL, mixed-lineage leukemia; PTD, partial tandem duplication.

**Conflict of interest:** The authors have declared that no conflict of interest exists.

**Citation for this article:** *J. Clin. Invest.* **116**:2707–2716 (2006). doi:10.1172/JCI25546.

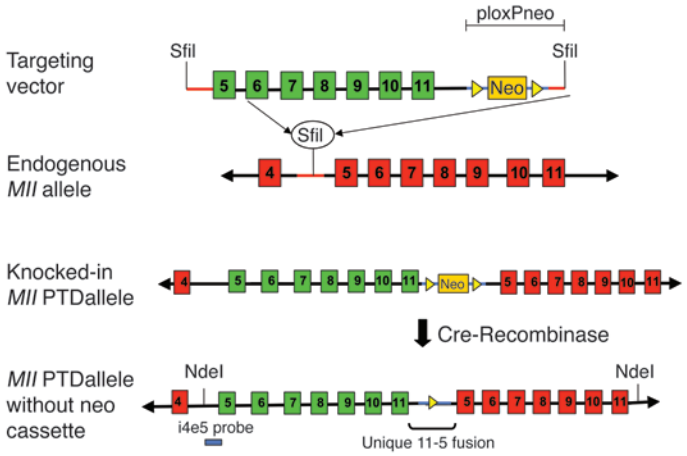


**Figure 1**
Generation of *Mll*$^{PTD/WT}$ mice. The backbone of the targeting vector is ploxPneo1 and contains a genomic clone spanning *Mll* intron 4 through intron 11. Linearization of the vector at a unique SfiI site within intron 4 allows for recombination at the germline intron 4 of *Mll*. A plasmid vector expressing Cre recombinase from a CMV promoter (pCre) was used to excise the neo cassette.

be essential for normal MLL function and regulation. Absence or downregulation of taspase 1 leads to absence or decreases in transcription of normal downstream targets of MLL, such as the *Hox* genes (12). In virtually all cases involving reciprocal *MLL* translocations, the consensus sequences for taspase 1 are lost and replaced by the fusion partner, resulting in one of the only known common features among all the reciprocal translocations involving *MLL*. However, the MLL PTD differs from translocations in that the consensus sequences for taspase 1 are retained and the MLL PTD protein is cleaved (13). How these MLL mutations function with or without taspase 1 cleavage is currently unsolved but highlights another important difference between MLL fusions and the MLL PTD.

In this study, we created a mouse expressing the *Mll* PTD off of the endogenous *Mll* promoter and examined the molecular basis for its phenotype. We show that this mouse has overexpression of certain *HoxA* genes, axial skeletal defects, and aberrant hematopoiesis, all compared with age- and sex-matched littermate controls. We also show that the *Mll* PTD is associated with increased histone H3/H4 acetylation and methylation of H3 Lys4 at *cis*-regulatory *HoxA* sequences, providing what we believe to be the first in vivo evidence for a mechanism by which an *MLL* gene rearrangement can directly alter *HoxA* gene expression.

## Results

*Mll*$^{PTD/WT}$ *mice are viable and express the fusion transcript*. To study the in vivo consequences of the *Mll* PTD and to more closely model the monoallelic involvement seen in human AML with the *MLL* PTD (14), we employed homologous recombination in ES cells to introduce a genomic fragment containing exons 5 through 11 into intron 4 of *Mll* (Figure 1). Using 2 *Mll*$^{PTD/WT}$(+) ES clones, we obtained 11 mice with germline transmission of the *Mll* PTD and backcrossed these mice with C57BL/6J mice to obtain *Mll*$^{PTD/WT}$ mice on a pure (congenic) C57BL/6J background. Southern blotting (Figure 2A) and DNA PCR (not shown) verified the presence of the *Mll*$^{PTD/WT}$ genotype. Southern blotting on 1-day-old pups from 5 matings also confirmed that *Mll*$^{PTD/PTD}$ homozygous mice are embryonic lethal (Table 1). Sequencing of the RT-PCR product from *Mll*$^{PTD/WT}$ mice demonstrated a correctly spliced, in-frame fusion transcript confirming the precise targeting of exons 5 through 11 within intron 4 of the *Mll* locus (Figure 2B).

*Absolute quantification of WT and PTD transcripts in Mll*$^{PTD/WT}$ *mice using real-time RT-PCR*. Real-time primers and probes were designed and optimized, amplifying the unique 11-5 *Mll* PTD fusion present only in *Mll*$^{PTD/WT}$ mice as well as the 14-15 *Mll* exon-exon junction located outside the duplicated region and common to both the *Mll* PTD allele and the *Mll* WT allele. Using these probes in an absolute quantification assay (13), it was determined that the *Mll* PTD and *Mll* WT alleles were both expressed at low, near equivalent levels in the hematopoietic tissues of the *Mll*$^{PTD/WT}$ mice (Figure 3 and Table 2). Protein confirmation of this equal yet low level of gene expression by Western blot was not technically possible.

*Phenotypic abnormalities of Mll*$^{PTD/WT}$ *mice*. Examination of *Mll*$^{PTD/WT}$ mice revealed skeletal abnormalities compared with *Mll*$^{WT/WT}$ age- and sex-matched littermate controls. Radiographic examination

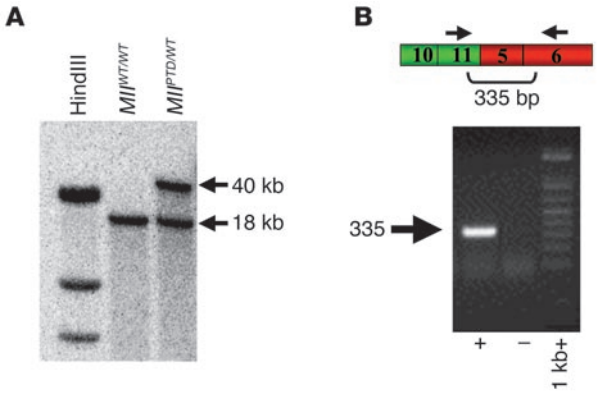


**Figure 2**
Germline transmission and verification of correct targeting in mice heterozygous for the *Mll* PTD. (**A**) Southern blot analysis using high molecular-weight DNA from spleens, digested with NdeI and hybridized to a probe that spans intron 4 and exon 5 of *Mll* (i4e5 in Figure 1). This generates a single WT band at 18 kb in *Mll*$^{WT/WT}$ mice, 2 bands representing 1 WT allele at 18 kb, and a band at 40 kb representing the rearranged allele in *Mll*$^{PTD/WT}$ mice. (**B**) The *Mll* PTD fusion transcript was amplified using an upstream primer from *Mll* exon 11 and a downstream primer from *Mll* exon 6 amplifying a single 335-bp unique fusion transcript in the *Mll*$^{PTD/WT}$ mouse (+) and is absent in the sample from the *Mll*$^{WT/WT}$ mouse (–). Sequencing of these PCR products from the *Mll*$^{PTD/WT}$ mice verified the presence of the exon 11–exon 5 fusion site. The 1-kb+ ladder was used to determine amplification size.

**Table 1**
Assessment of Mendelian ratios for the *Mll* PTD allele

| Matings | Matings (no.) | Total $Mll^{WT/WT}$ offspring (expected freq/actual freq)[A] | Total $Mll^{PTD/WT}$ offspring (expected freq/actual freq) | Total $Mll^{PTD/PTD}$ offspring (expected freq/actual freq) |
|---|---|---|---|---|
| $Mll^{PTD/WT} \times Mll^{PTD/WT}$ | 5 | 8 (25:30) | 19 (50:70) | 0 (25:0) |

[A]All ratios in parentheses indicate percentages. Freq, frequency.

of $Mll^{PTD/WT}$ mice less than 1 year of age identified axial skeleton malformations, including a rudimentary or missing thirteenth rib, indicative of a T13→L1 transformation (70% penetrance, $n = 13$), and an S1 vertebral duplication, indicative of an S2→S1 transformation (63%, $n = 11$) (Figure 4, B and C).

Given the WT Mll's role in maintaining *Hox* expression during development and the known association between *HoxA* expression, anteroposterior patterning, and posterior axis elongation, we examined *Hoxa9* expression during embryogenesis. In situ hybridization performed on E12.5 $Mll^{PTD/WT}$ embryos demonstrated a shifted expression boundary of *Hoxa9* within the paraxial mesoderm compared with $Mll^{WT/WT}$ littermate controls (Figure 5).

*Altered hematopoiesis in $Mll^{PTD/WT}$ mice is associated with aberrant HoxA expression*. Lineage-specific CFU assays were performed for erythroid (measured by erythropoietic burst formation [BFU-E]), myeloid, (measured by GM-CFU), and mixed (measured by granulocyte, erythroid, macrophage, megakaryocyte–CFU [GEMM-CFU]) progenitor populations, using both $Mll^{PTD/WT}$ and $Mll^{WT/WT}$ splenocytes. The CFU number for each progenitor type was significantly increased in $Mll^{PTD/WT}$ mice compared with age- and sex-matched $Mll^{WT/WT}$ littermate controls (Figure 6A). A 5- to 20-fold increase in $Mll^{PTD/WT}$ spleen cells expressing the erythroid marker Ter119 was also noted, consistent with the observed increase in erythroid progenitor populations as measured by BFU-E (Figure 6, B and C). However, extensive phenotypic analyses performed as previously described (15) on blood, spleen, and BM did not reveal any other differences in $Mll^{PTD/WT}$ mice compared with age- and sex-matched $Mll^{WT/WT}$ littermate controls (see representative flow cytometric analyses, Supplemental Figure 1; available online with this article; doi:10.1172/JCI25546DS1). Primary CFUs were then harvested and used in 2 parallel secondary assays. In replating CFU assays, the total number of colonies per plate was not significantly different between $Mll^{PTD/WT}$ and $Mll^{WT/WT}$ splenocytes, yet the size of the $Mll^{PTD/WT}$ colonies was markedly increased over both $Mll^{WT/WT}$ colonies and those derived from $Mll^{Af9/WT}$ mice (Figure 6, D–F). Secondary colonies from $Mll^{PTD/WT}$ mice were able to form tertiary and quaternary colonies while those from $Mll^{WT/WT}$ and $Mll^{Af9/WT}$ mice were not (data not shown). The increase in size per $Mll^{PTD/WT}$ colony suggested an increase in progenitor cell proliferation compared with $Mll^{WT/WT}$ progenitor cells. Nonetheless, absolute in vivo cell counts in bone marrow, spleen, and blood were not significantly different between $Mll^{PTD/WT}$ and $Mll^{WT/WT}$ mice, suggesting that enhanced proliferation in the $Mll^{PTD/WT}$ progenitor cells was accompanied by increased cell turnover. To verify this, primary CFU colonies were harvested and maintained in liquid cultures supplemented with SCF, IL-3, and IL-6 for an additional 18 days, followed by cell counts, measurement of BrdU uptake for quantification of proliferation, and assessment of apoptosis by annexin V and propidium iodide staining. The $Mll^{PTD/WT}$ hematopoietic progenitor cells did have a 2-fold greater fraction of cells incorporating BrdU compared with $Mll^{WT/WT}$ progenitor cells (Figure 6, G–H) but also showed a substantial amount (50%) of apoptosis (Figure 6I) such that absolute cell counts over this period of time were only modestly increased from the initiation of culture (Table 3). This near maintenance of homeostasis could also explain the normal cell counts observed in bone marrow, spleen, and blood of $Mll^{PTD/WT}$ mice in vivo. The lack of viable $Mll^{WT/WT}$ cells at day 18 in repeated assays (Table 3) precluded our ability to obtain statistically meaningful comparative data in repeated cultures. In contrast, $Mll^{PTD/WT}$ progenitor cells were sustained in liquid culture for more than 4 months.

*Increased expression of HoxA genes in $Mll^{PTD/WT}$ mice*. To establish a possible cause for the aberrant increases in both the number of primary colonies and increased proliferative capacity of replated progenitors from $Mll^{PTD/WT}$ mice, we quantified expression of *Hoxa7*, *Hoxa9*, and *Hoxa10* within hematopoietic tissues. We found consistent and significant overexpression of each *HoxA* gene in BM, spleen, and blood when compared with their expression in matched $Mll^{WT/WT}$ littermate controls (Figure 7, A–C). Expression of *Hoxa1*, a *HoxA* family member that is not regulated by *Mll,* was unaltered in any of the hematopoietic tissues examined while *Hoxc8*, a *HoxC* family member that has been shown to be positively regulated by WT MLL (8), was also not upregulated in any of the tissues examined (not shown).

The lack of significant differences in cellular populations of blood, spleen, and BM between $Mll^{PTD/WT}$ and $Mll^{WT/WT}$ mice as noted above suggested that the increased *HoxA* gene expression was due to an increase in the *HoxA* expression on a per cell basis. To confirm this, we sorted equal numbers of cells from BM of $Mll^{PTD/WT}$ and $Mll^{WT/WT}$ mice expressing different lineage markers: B220, CD3, CD11b, Gr-1, and Ter119. RNA was isolated from an equivalent number of cells and reverse transcribed into cDNA. Using real-time RT-PCR, *Hoxa9*

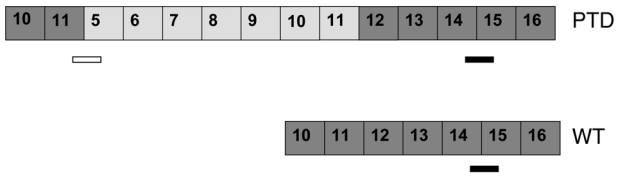


**Figure 3**
*Mll* WT and *Mll* PTD transcripts. Schematic demonstrating the real-time RT-PCR strategy for detection and absolute quantification of the *Mll* WT and *Mll* PTD transcripts in bone marrow and spleen of *Mll* PTD mice. The predicted *Mll* PTD and *Mll* WT allele–derived transcripts are shown, with the tandemly duplicated exons 5–11 present in the PTD transcript denoted with light gray boxes. Shown below the transcripts are sites for PCR primers and fluorogenic probes designed to amplify either the unique exon 11–exon 5 fusion (open rectangle) or exons 14–15, whose junction is common to the *Mll* WT and *Mll* PTD transcripts (filled rectangle).

**Table 2**
Absolute quantitation of *Mll* PTD and *Mll* WT transcripts

| Genotype | Copy no. *Mll* PTD amplicon (11-5 fusion) | Copy no. *Mll* common amplicon (14–15 exons) | Ratio | SD |
|---|---|---|---|---|
| $Mll^{PTD/WT}$ | 367 | 920 | 2.5[A] | 0.3 |
| $Mll^{WT/WT}$ | – | 2070 | – | – |

To determine whether the equivalent amount of transcript was being produced from each allele in the $Mll^{PTD/WT}$ tissues, the *Mll* PTD unique fusion amplicon copy number was subtracted from the common amplicon (shared between the *Mll* PTD and *Mll* WT alleles) copy number. [A]If both alleles were transcribed at equivalent rates, the common-to-unique amplicon copy number ratio would be approximately 2:1 in a sample with the $Mll^{PTD/WT}$ genotype or approximately 1:1 if the *Mll* WT allele was silenced (13). $n$ = 3/genotype.

was shown to be overexpressed in each of the $Mll^{PTD/WT}$ cell subsets when compared with the identical $Mll^{WT/WT}$ subset, consistent with an increase in *HoxA* gene expression on a per cell basis (Figure 7D).

*Epigenetic alterations at HoxA gene promoters in $Mll^{PTD/WT}$ mice.* As noted earlier, *HoxA* gene overexpression has been noted in both in vitro and in vivo models of the *MLL-AF9* fusion, but an in vivo mechanism to explain this upregulation in this or any *MLL* rearrangement associated with leukemia has yet to be provided (11). Two groups have shown that WT MLL has intrinsic histone H3 Lys4 methyltransferase activity within its C terminus SET domain (7, 8), which is retained in the *MLL* PTD. To test whether epigenetic modifications within *HoxA* promoters were responsible for *HoxA* overexpression in $Mll^{PTD/WT}$ hematopoietic tissues, chromatin immunoprecipitation (ChIP) was performed within promoter sequences known to be important for maintaining *HoxA* transcription and spleen and BM were compared with similar tissues in $Mll^{WT/WT}$ mice. $Mll^{PTD/WT}$ mice displayed an increase in histone H3 and H4 acetylation and H3 Lys4 methylation with a corresponding decrease in H3 Lys9 methylation within the *Hoxa9* (Figure 8, A and B) and *Hoxa7* (not shown) promoters. These epigenetic modifications associated with gene transcription establish a mechanistic link between the $Mll^{PTD/WT}$ genotype and the associated overexpression of *Mll* targets *Hoxa7* and *Hoxa9*. No such epigenetic changes were noted within the pertinent promoter region of *Hoxa10*.

We further assessed whether the increased histone modifications associated with gene activation were due to a gain of function of the *Mll* PTD and not the result of losing a WT *Mll* allele. H3/H4 acetylation and H3 Lys4 methylation at the *Hoxa7* and *Hoxa9* promoters were therefore measured using ChIP in combination with SYBR green real-time PCR in $Mll^{PTD/WT}$ and $Mll^{WT/-}$ BM and spleen and compared with similar measurements in $Mll^{WT/WT}$ BM and spleen. Results show no significant difference in the histone modifications at these promoters when comparing $Mll^{WT/-}$ and $Mll^{WT/WT}$ tissues. In contrast, $Mll^{PTD/WT}$ tissues showed significantly increased H3/H4 acetylation and H3 Lys4 methylation at the *Hoxa7* and *Hoxa9* promoters when compared with these other 2 genotypes (Figure 8, C and D, and Table 4). These data indicate that the histone modifications associated with gene activation in the $Mll^{PTD/WT}$ cells result from gain-of-function mutation involving the PTD and not simply the loss of a WT *Mll* allele. It should also be noted that *HoxA* gene expression in $Mll^{PTD/WT}$ E17.5 fetal liver cells showed a 5- to 10-fold increase in *Hoxa7*, *Hoxa9*, and *Hoxa10* gene expression compared with either $Mll^{WT/WT}$ or $Mll^{WT/-}$ fetal liver cells (data not shown). Finally, preliminary experiments comparing fetal liver cell *HoxA* gene expression obtained from $Mll^{PTD/WT}$, $Mll^{WT/-}$, and $Mll^{PTD/-}$ E17.5 embryos strongly support the conclusion that the *Mll* PTD confers a gain-of-function mutation (A. Dorrance and M. Caligiuri, unpublished observations).

*Absence of leukemic transformation in $Mll^{PTD/WT}$ mice highlights important requirement for second hit in the progression of leukemia.* Despite the aberrant hematopoiesis, the mice had not developed leukemia over 2 years of observation. Hoxa9 cooperates with overexpressed Meis1 in the induction of murine AML (16–18). We therefore quantified *Meis1* transcript in affected hematopoietic tissues but found no evidence of overexpression (not shown). Likewise, we have noted that AML blasts from patients harboring the *MLL* PTD consistently lack expression of the WT *MLL* allele (13); however, hematopoietic tissues of $Mll^{PTD/WT}$ mice showed near equivalent levels of WT and PTD transcript (Figure 2C). Thus, it is possible that these and/or other additional molecular alterations are required for malignant transformation and can explain the aberrant hematopoiesis in the absence of leukemic transformation in $Mll^{PTD/WT}$ mice.

## Discussion

In the current report, we describe a mouse engineered with *Mll* PTD expression driven by its endogenous promoter. The $Mll^{PTD/PTD}$ genotype appears embryonic lethal, and characterization of these

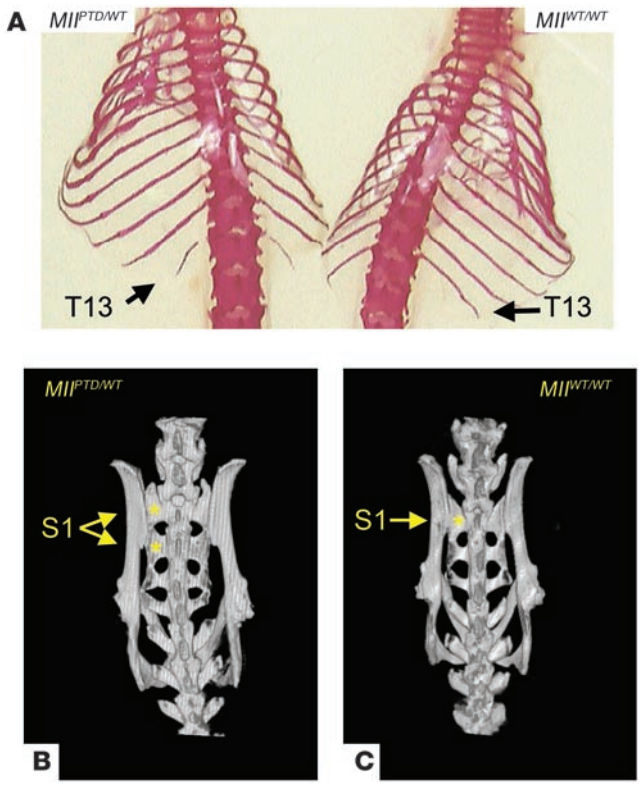


**Figure 4**
Skeletal analysis of $Mll^{PTD/WT}$ mice at 20 weeks of age. (**A**) Alizarin red staining of $Mll^{PTD/WT}$ (left) and $Mll^{WT/WT}$ (right) mice shows a rudimentary/missing thirteenth rib, indicative of a T13 → L1 transformation (penetrance of 70% in $Mll^{PTD/WT}$ mice, $n$ = 13). MicroCT images of the sacral spine in a (**B**) $Mll^{PTD/WT}$ mouse and a (**C**) $Mll^{WT/WT}$ mouse in 3D. These images are viewed from the dorsal side and illustrate the duplication of the S1 vertebral body, indicative of an S2→S1 transformation in the $Mll^{PTD/WT}$ mice (penetrance of 63%, $n$ = 11).

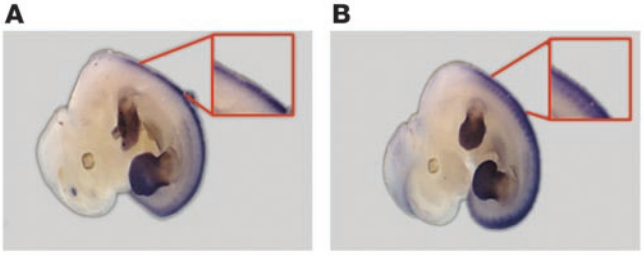


**Figure 5**
In situ hybridizations for *Hoxa9* on E12.5 embryos. (**A**) $Mll^{WT/WT}$ and (**B**) $Mll^{PTD/WT}$ embryos hybridized with a digoxygenin-labeled probe for *Hoxa9*. Results demonstrate a notable ventral shift of the *Hoxa9* expression boundary within the paraxial mesoderm of the $Mll^{PTD/WT}$ embryo compared with the $Mll^{WT/WT}$ littermate control (see inset for each figure). This figure represents 1 of 3 comparable hybridizations.

embryos is ongoing. $Mll^{PTD/WT}$ mice are viable, are able to reproduce, and are without serious illness after 2 years of observation. However, $Mll^{PTD/WT}$ mice have a high penetrance of skeletal abnormalities that consist of a missing or rudimentary thirteenth rib and a duplication of the S1 vertebral body.

Hematopoietic abnormalities consist of significantly increased BFU-E, GM-CFU, and GEMM-CFU progenitors in cultures from $Mll^{PTD/WT}$ splenocytes when compared with age- and sex-matched $Mll^{WT/WT}$ littermate controls. Alterations in members of the homeobox or *Hox* family of genes could reasonably explain these seemingly diverse phenotypic findings in the *Mll* PTD mice since certain *Hox* members are critical in axioskeletal and hematopoietic development and maintenance of *Hox* expression is positively regulated by WT *Mll* (1). The current report documents the increased expression of selected *HoxA* genes that is coincident with the *Mll* PTD and, for what we believe is the first time, provides a mechanism by which an *Mll* defect that is associated with AML causes deregulation of *HoxA* expression in vivo.

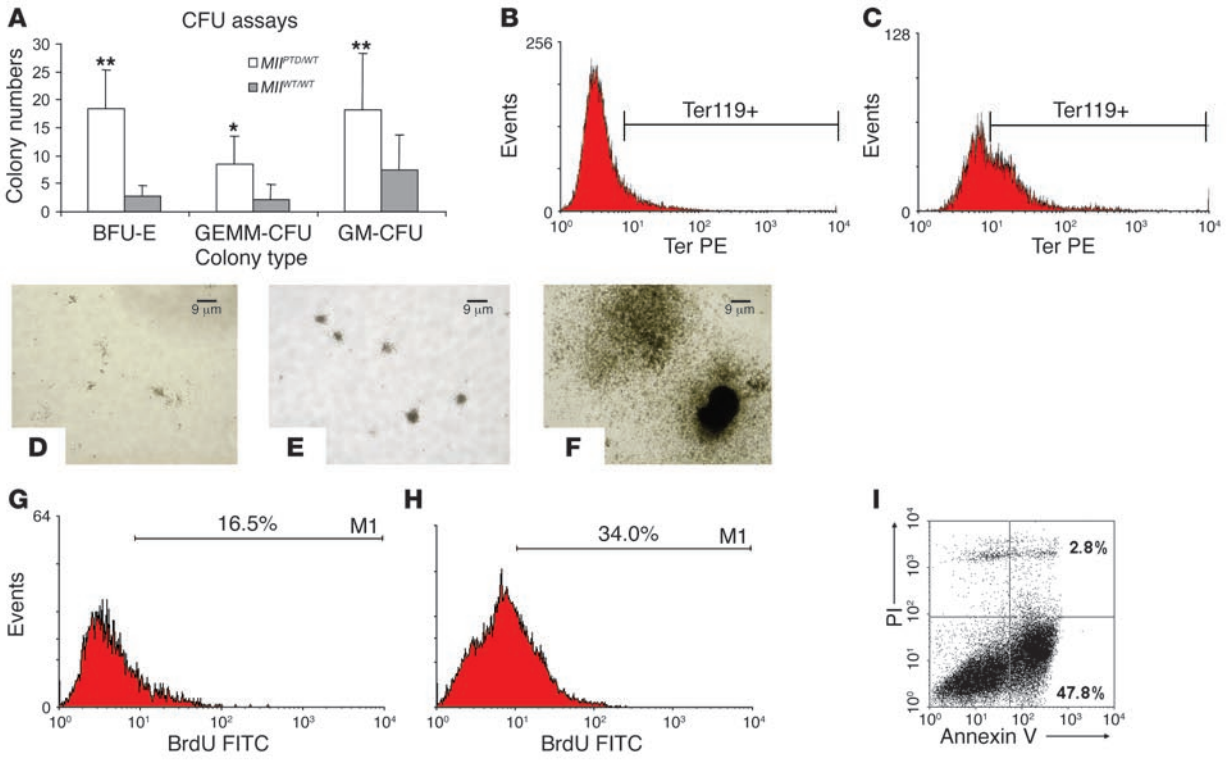


**Figure 6**
Evaluation of progenitor populations in $Mll^{PTD/WT}$ splenocytes compared with $Mll^{WT/WT}$ sex-matched littermate controls. (**A**) Results from CFU assays to assess progenitors of erythroid (BFU-E), granulocytic, erythroid, monocytic, megakaryocytic (GEMM-CFU), and granulocyte, macrophage (GM-CFU) lineages show significantly increased CFUs derived from $Mll^{PTD/WT}$ versus $Mll^{WT/WT}$ splenocytes. *$P = 0.03$; **$P = 0.0025$. Error bars indicate SD. Splenocytes from (**B**) $Mll^{WT/WT}$ and (**C**) $Mll^{PTD/WT}$ mice ($n = 8$ mice per genotype) show increased surface density expression of the erythroid marker Ter119 in $Mll^{PTD/WT}$ mice. Ter PE, PE fluorochrome–conjugated Ter119. Secondary splenic colonies from (**D**) $Mll^{WT/WT}$, (**E**) $Mll^{Af9/WT}$, and (**F**) $Mll^{PTD/WT}$ mice ($n = 6$ mice per genotype, plated in duplicate). The numbers of secondary colonies per plate (~230) were similar between genotypes. The number of cells per colony was dramatically increased in $Mll^{PTD/WT}$ mice compared with $Mll^{WT/WT}$ or $Mll^{Af9/WT}$ mice. (**G**–**I**) Primary CFU progenitor cells harvested after 14 days and maintained in liquid cultures for 18 days, supplemented with SCF, IL-3, and IL-6, and in the presence of BrdU for the last 4 days. An anti-BrdU antibody gated on viable cells demonstrates a smaller fraction of $Mll^{WT/WT}$ cells proliferating (**G**) compared with $Mll^{PTD/WT}$ cells (**H**). Assessment of programmed cell death (**I**, upper right and lower right quadrants) revealed a sizeable fraction (~50%) of $Mll^{PTD/WT}$ progenitors undergoing apoptosis during expansion. While a significant fraction of $Mll^{PTD/WT}$ cells were proliferating, approximately 50% were undergoing apoptosis. In 2 additional experiments, the $Mll^{WT/WT}$ cells had already died by this time point in culture (see Table 3), precluding a statistical comparison of these results in **G**–**I**.

**Table 3**
Splenic progenitor cells grown in liquid culture

| Genotype | Day 0[A] (no. cells) | Day 7 (no. cells) | Day 18 (no. cells) |
|---|---|---|---|
| $Mll^{WT/WT}$ | $2.2 \times 10^6$ | $1.2 \times 10^5$ | $1.3 \times 10^4$ (↓) |
| $Mll^{WT/WT}$ | $7.5 \times 10^4$ | All dead | All dead |
| $Mll^{WT/WT}$ | $9.9 \times 10^5$ | $6.9 \times 10^5$ | All dead |
| $Mll^{PTD/WT}$ | $6.2 \times 10^6$ | $1.3 \times 10^6$ | $7.5 \times 10^6$ (↑) |
| $Mll^{PTD/WT}$ | $3.7 \times 10^6$ | $1.2 \times 10^6$ | $1.5 \times 10^7$ (↑) |
| $Mll^{PTD/WT}$ | $6.0 \times 10^6$ | $1.9 \times 10^6$ | $8.7 \times 10^6$ (↑) |

[A]Signifies the start of liquid cultures with cells harvested from day 14 CFUs. Arrows indicate increase or decrease in number of cells at day 18 compared with day 7.

*Hox* genes display spatiotemporal expression patterns that are colinear with respect to their location on the chromosome (19). Thus, for normal skeletal development to proceed, *Hox* genes must be expressed in the right cell type at the right time. Expression of these genes at incorrect times or locations leads to disruptions in normal *Hox* expression boundaries, resulting in altered cell fate and misspecification of segment identities (20–22). To determine whether the malformations of the axial skeletons of our $Mll^{PTD/WT}$ mice were associated with alterations in *Hox* expression boundaries, we performed whole-mount in situ hybridizations on E12.5 embryos and found the expression of *Hoxa9* in the $Mll^{PTD/WT}$ embryos extended laterally in the somitic mesoderm when compared with $Mll^{WT/WT}$ littermate controls. This finding is consistent with other reports that have implicated *Hoxa9* as an important gene for lumbosacral patterning (23).

Restricted *Hox* expression is also vital for normal hematopoiesis, and deregulation in *HoxA* expression can result in aberrant hematopoiesis and malignant transformation (18, 24–30). Following the observations of progenitor cell abnormalities in $Mll^{PTD/WT}$ spleen, we noted significant increases in *Hoxa7, Hoxa9*, and *Hoxa10* transcripts in the spleen, BM, and blood of $Mll^{PTD/WT}$ mice when compared with $Mll^{WT/WT}$ littermate controls and with $Mll^{WT/-}$ mice. However, *Hoxa1*, a *HoxA* family member not regulated by *Mll*, showed no increase in its expression in tissues of the $Mll^{PTD/WT}$ mice. Likewise, *Hoxc8*, a member of the HoxC paralogous group that has been shown to be a direct target of MLL, was not increased within these tissues, indicating the specific effect of the Mll PTD on these *HoxA* genes. Further, as these *HoxA* family members are positively regulated by WT Mll, their consistent and significant overexpression in the tissues of $Mll^{PTD/WT}$ mice also suggests that the Mll PTD was operating in a gain-of-function fashion.

WT MLL has been shown to directly and indirectly modify histones at the promoters of certain *HOX* genes, thereby maintaining gene transcription (7, 8). Histone modifications are associated with gene activation and repression (31–33). Histone acetylation is the predominant modification associated with gene activation as well as histone H3 Lys4 methylation, while histone H3 Lys9 methylation corresponds with gene repression. Enzymes

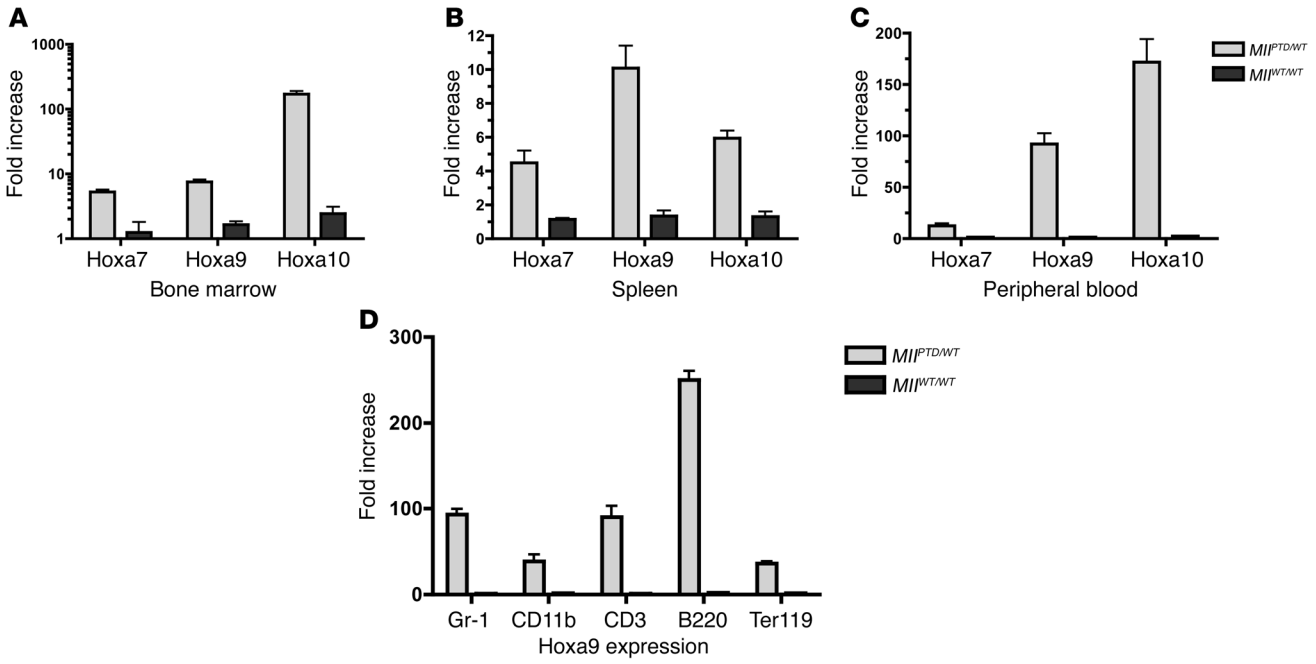


**Figure 7**
*HoxA* gene expression levels. (**A**–**C**) Quantification of *Hoxa7, Hoxa9,* and *Hoxa10* expression in hematopoietic tissues of $Mll^{WT/WT}$ and $Mll^{PTD/WT}$ mice. Cells were isolated from (**A**) BM, (**B**) spleen, and (**C**) blood from both $Mll^{WT/WT}$ and $Mll^{PTD/WT}$ mice ($n$ = 10 mice per genotype). RNA and then cDNA were prepared and quantified by real-time RT-PCR. $Mll^{PTD/WT}$ mice showed increased expression of each of these *HoxA* genes in all 3 tissues compared with sex-matched littermate $Mll^{WT/WT}$ mice. (**D**) Equal numbers of each sorted BM population expressing Gr-1, CD11b, CD3, B220, or Ter119 from $Mll^{PTD/WT}$ mice and $Mll^{WT/WT}$ mice were processed for RNA and then cDNA. Absolute quantification of *Hoxa9* expression was then determined by real-time RT-PCR and demonstrated that $Mll^{PTD/WT}$ cells have increased *Hoxa9* expression within each population compared with the equivalent number of $Mll^{WT/WT}$ cells, indicating that *Hoxa9* transcript levels are overexpressed on a per cell basis (values shown represent mean of $n$ = 3 mice per genotype ± SD; $P < 0.03$).

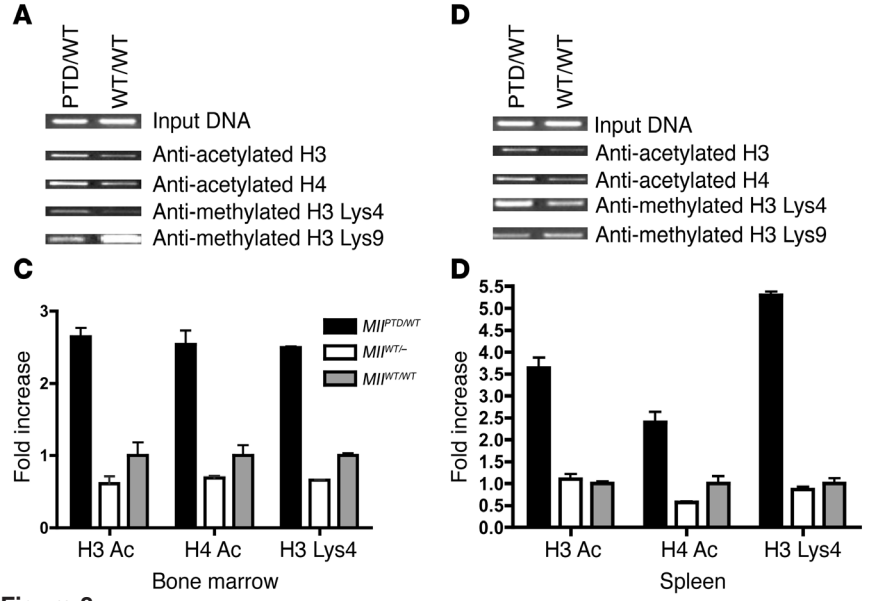


**Figure 8**

Assessment of Mll target gene *Hox*a9 acetylation and methylation of histones assessed by ChIP using (**A**) bone marrow cells and (**B**) splenocytes derived from $Mll^{PTD/WT}$ and $Mll^{WT/WT}$ mice. Results show an increase at the *Hoxa9* promoter in histone H3/H4 acetylation as well as histone H3 Lys4 methylation and a corresponding decrease in histone H3 Lys9 methylation in $Mll^{PTD/WT}$ bone marrow and spleen compared with the same $Mll^{WT/WT}$ tissues. Results are representative of 3 independent experiments. Similar results were obtained at the *Hoxa7* promoter but were not seen at the *Hoxa10* promoter (not shown). (**C**) BM cells and (**D**) splenocytes derived from $Mll^{PTD/WT}$, $Mll^{WT/–}$, and $Mll^{WT/WT}$ mice. Absolute quantification by SYBR green real-time PCR shows a significant increase at the *Hoxa9* promoter in histone H3/H4 acetylation as well as histone H3 Lys4 methylation in $Mll^{PTD/WT}$ BM and spleen compared with the same $Mll^{WT/–}$ and $Mll^{WT/WT}$ tissues ($n = 3$ mice per genotype; $P < 0.05$). There was no significant difference between $Mll^{WT/–}$ and $Mll^{WT/WT}$ tissues.

known as histone acetyltransferases, such as cAMP response element–binding protein–binding protein (CBP), are responsible for histone acetylation and associate with MLL in a complex via its C terminal transactivation domain, which is uniquely preserved in the MLL PTD (34). There are genetic data showing evolutionarily conserved association of the MLL homolog Trx with *Drosophila* CBP in the fly, thus demonstrating the importance of this protein interaction (35). Other complexes found within the MLL supercomplex function as either activators or repressors of transcription, some via acetylation (7, 8). Examination of the histone acetylation states at *Hoxa7* and *Hoxa9* promoters in our study showed overacetylation of histone H3/H4 in spleen and BM of $Mll^{PTD/WT}$ mice, explaining at least 1 mechanism by which the *Mll* PTD is mediating *HoxA* overexpression. The specific complexes associating with the *Mll* PTD that are responsible for this observation and the direct or indirect mechanism by which this is accomplished have yet to be elucidated.

Like the transactivation domain, the SET domain is also retained in the C terminus of the MLL PTD, again in contrast to all other *MLL* gene fusions found in AML. The SET domain of MLL has histone H3 Lys4 methyltransferase activity essential for maintaining *Hox* expression (7, 8). We hypothesized that histone H3 Lys4 methylation might also contribute to upregulation of these *HoxA* genes. Indeed, ChIP experiments revealed a correlation between overexpression of both *Hoxa7* and *Hoxa9* transcript with increases of histone H3 Lys4 methylation at these promoters in $Mll^{PTD/WT}$ tissues. These data and the absence of such an increase in the same tissues of $Mll^{WT/–}$ mice support the notion that the *Mll* PTD has a direct gain-of-function role in transcriptional activation of these target genes.

In contrast, the retroviral infection of $Mll^{–/–}$ murine embryonic fibroblasts with the *MLL-AF9* fusion (lacking the SET domain) did not result in comparable *Hoxa9* promoter modifications despite overexpression of the *Hoxa9* transcript (7, 8). Transductions using the MLL–*eleven nineteen leukemia* and MLL–*FK506-binding protein* fusions demonstrated binding to *HoxA* promoters and increases in H3 acetylation but no corresponding increases in H3 Lys4 methylation (36). These experiments suggest distinct mechanisms of action in which *Hoxa9* is positively regulated by different *MLL* gene fusions. In addition, our ChIP experiments showed a correlation between the overexpression of *Hoxa7* and *Hoxa9* and a decrease in the repression-associated methylation of histone H3 Lys9 at each promoter; however, the domain and/or complex within the *Mll* PTD that is associated with this epigenetic modification is unknown. Interestingly, we did not find similar histone modifications at the *Hoxa10* promoter, suggesting its mechanism of overexpression is distinct from those we observed in *Hoxa7* and *Hoxa9* in $Mll^{PTD/WT}$ mice.

Exactly how the associated aberrant epigenetic modifications come about is unknown but must be directly or indirectly related to the PTD itself. Several possible mechanisms are now conceivable with the recent evidence that WT MLL directly binds to the promoter of these *HoxA* target genes, together with its supercomplex of repressing and activating proteins (7, 8). The duplication of the DNA-binding AT-hook DNA-binding domain within the Mll PTD may have conferred sustained and therefore excessive binding and increased activation at the relevant *Hoxa7* and *Hoxa9* promoters or could in some way enhance the recruitment of the *Mll* PTD and its supercomplex to its target genes (37). Alternatively, the associated supercomplex of activating and repressing components may be altered by the PTD in a way that changes a critical balance between these various complexes, excessively favoring target gene activation. It is conceivable that the binding of the Mll PTD to the promoter of these *HoxA* genes may interfere with the recruitment of the repression machinery. Careful biochemical characterization of these regulatory regions within the promoters of downstream targets of Mll will provide further insights into the dynamic regulation of these gene products in vivo.

Retroviral overexpression of *Hox* genes, including *HoxA* members, has been associated with massive deregulation of hematopoiesis and leukemia (27). Despite the sometimes substantial overexpression of the same *HoxA* genes observed in our $Mll^{PTD/WT}$ mice, they displayed no signs of malignant transformation at 2 years of age. The increase in $Mll^{PTD/WT}$ progenitor cell number and proliferation during CFU and liquid culture assays, respectively, suggests that *HoxA* overexpression exerts

**Table 4**
Assessment of *Mll*$^{PTD/WT}$ and *Mll*$^{WT/-}$ phenotypes compared with *Mll*$^{WT/WT}$ genotype

| Phenotype | *Mll*$^{PTD/WT}$ [A] | *Mll*$^{WT/-}$ |
|---|---|---|
| **Axial skeleton** | | |
| | S1 sacral duplication<br>No cervical abnormalities | No sacral abnormalities[B]<br>Multiple cervical abnormalities[B] |
| **Hematopoiesis** | | |
| | Normal blood volume<br>Normal numbers of normal B cell populations | Anemia[B]<br>Normal or decreased B cell populations[B] |
| ***Mll* Function** | | |
| | Significantly increased H3/H4 acetylation and<br>H3 Lys4 methylation at Hoxa7 and Hoxa9 promoters[C] | Normal or decreased[A,C] |

[A]Determined in our laboratory. [B]Reported by Yu et al. (1). [C]See Figure 8, C and D.

its effect on immature cells of the hematopoietic compartment but by itself is insufficient to cause leukemic transformation. Overexpression of *Hoxa7* or *Hoxa9* rapidly induces AML in mice but requires forced coexpression of the *Hox* cofactor *Meis1* (16). *Mll*$^{PTD/WT}$ cells overexpressing *Hoxa7* and *Hoxa9* genes in our study did not display any increase in *Meis1* transcript. Further, AML patients harboring the *MLL* PTD also undergo epigenetic silencing of their WT *MLL* allele in their leukemic blasts that contributes to enhanced cell survival (13). Our *Mll* PTD mice express the WT *Mll* allele, presumably because this later event requires cooperation with other alterations. Finally, the *MLL* PTD has been shown to occur simultaneously with tyrosine kinase mutations in AML, such as the FLT3 ITD (38) and Rhe-PDGFRα fusion (39), neither of which has been detected in our *Mll*$^{PTD/WT}$ mice. Thus, the failure of our mice to develop frank leukemia is likely related to the absence of additional molecular aberrations that are critical for malignant transformation to occur in the presence of the *Mll* PTD.

While it would seem most logical that we are observing the earliest events in a continuum of how the *Mll* PTD contributes to the leukemic phenotype, it must also be considered that some or all of the abnormalities we have observed may not be related to the leukemogenic process as it occurs in patients with AML and the *MLL* PTD. For example, while the excessive production of erythroid and megakaryocytic progenitor populations is consistent with the specific role of *Hoxa10* in these lineages (28) and with *Hoxa10* overexpression found in the *Mll*$^{PTD/WT}$ mice, AML patients with the *MLL* PTD rarely have blasts of erythroid or megakaryocyte lineage. Clearly, additional work in combination with mice harboring other genetic defects, as described above, will need to be undertaken in order to shed light on the role of the *Mll* PTD in the genesis of leukemia.

In summary, we have engineered a mouse with the *Mll* PTD driven off of its endogenous promoter. We provide what we believe to be the first in vivo evidence for a mechanism by which an *Mll* gene fusion (in this case, a self fusion) strongly associated with AML leads to aberrant target gene activation, i.e., increased histone H3/H4 acetylation and histone H3 Lys4 methylation.

## Methods

All primers and primer/probe sets used, along with conditions of amplification can be found in Supplemental Tables 1 and 2.

*Development of the Mll*$^{PTD/WT}$ *mouse.* A P1 genomic clone containing the murine *Mll* genomic fragment was obtained from Incyte (formerly Genome Systems). This was subcloned as 2 fragments (F1 and F2) into pBluescript II as BamHI fragments. The BamHI/SmeI fragment from F2 was then subcloned into the BamHI and SmeI sites of ploxPneo1. F1 was then subcloned into the BamHI site of ploxPneo containing F2. This generated a targeting vector with ploxPneo1 as the vector backbone and genomic *Mll* sequences spanning intron 4 through intron 11 (Figure 1). All animal research was reviewed and approved by the Institutional Laboratory Animal Care and Use Committee at the Ohio State University.

Approximately 60 μg of the targeting vector was linearized within intron 4 of *Mll* using the unique *Sfi*I restriction site and introduced into $3 \times 10^7$ R1 ES cells. A plasmid vector expressing Cre recombinase from a CMV promoter (pCre) that conferred puromycin resistance was transiently transfected into C186 *Mll*$^{PTD/WT}$ ES cells by electroporation. Cells were cultured overnight and then transferred to a selective media containing 1 μg/ml of puromycin, grown further, and subcloned. Following transient transfection, selection, and expansion, DNA-PCR was performed using an upstream primer from intron 11 and a downstream primer from the ploxPneo vector. This amplified a 0.9-kb band, suggesting that the pgk-neo cassette had been removed, and this was confirmed by sequencing. Next, 2 independently targeted ES cell clones were selected for generating chimeric mice. After verifying that these clones were karyotypically normal and free of mycoplasma contamination, 15 ES cells from each clone were injected into 3.5-day-old blastocysts from pregnant C57BL/6 female mice (The Jackson Laboratory). Next, the chimeric embryos were transferred into pseudopregnant recipient Swiss-Webster female mice. Micromanipulations, blastocyst transfers, and generation of chimeric mice were performed at the Transgenic Shared Resource of The Ohio State University Comprehensive Cancer Center. Backcrossing to a pure C57BL/6 background was carried out in 5 generations using marker-assisted breeding (speed congenics) (The Jackson Laboratory).

*Southern blot analysis.* High molecular weight DNA extracted from cells was digested with SbfI and NdeI (New England Biolabs Inc.), and Southern blotting was performed according to previously described techniques (40). DNA was transferred to Hybond N+ nitrocellulose membrane (Amersham Biosciences) and hybridized to a cDNA fragment spanning the *Mll* intron 4–exon 5 junction. The predicted fragment size for the *Mll* PTD allele was 40 kb while the predicted fragment size for the WT *Mll* allele was 18 kb.

*Genotyping.* DNA was prepared from tail biopsies of adult and newborn mice using standard phenol/chloroform extraction. DNA PCR was performed using a forward primer located within intron 6 and a reverse primer located within the targeting vector backbone that amplifies a 900-bp product. Total RNA was extracted from tissues using the RNeasy Mini Kit (QIAGEN), and RT-PCR was performed using MMLV Reverse Transcriptase (Invitrogen) with a forward primer located within exon 11 and a reverse primer located within exon 6, which resulted in the generation of a 335-bp PCR product.

*CFU progenitor assays and liquid stem cell cultures*. Splenocytes were isolated from $Mll^{PTD/WT}$, $Mll^{WT/WT}$, and $Mll^{af9/WT}$ mice (generously provided by T. Rabbitts, Medical Research Council Laboratory of Molecular Biology, Cambridge, United Kingdom, via J. Kersey, Cancer Center, University of Minnesota, Minneapolis, Minnesota, USA). Single-cell suspensions were prepared in Iscove's Modified Dulbecco's Medium (Invitrogen) containing 2% of FBS (HyClone) from $n$ = 6–8 mice per genotype. Cells were then plated at a density of $2 \times 10^4$ cells/dish in M3434 methylcellulose (StemCell Technologies) to assess splenic progenitor populations. All colony assays were performed according to the manufacturer's protocol (StemCell Technologies). Secondary replating assays were enumerated and performed on day 14 of primary cultures. Cells were replated at a density of $10^4$ cells/dish in M3434 methylcellulose (StemCell Technologies). Secondary cultures were also performed in liquid medium RPMI 1640 with GlutaMAX (Invitrogen) plus 100 ng/ml of stem cell factor, 10 ng/ml of mouse IL-3, and 20 ng/ml of human IL-6 (StemCell Technologies) and seeded simultaneously from primary CFU progenitor assays and in parallel with secondary replating assays at a density of $10^4$ cells/ml.

*ChIP*. ChIP assays were performed using the Chromatin Immunoprecipitation Assay Kit (Upstate USA Inc.). Approximately $3 \times 10^6$ cells were used per assay, and approximately 1% of the extracted chromatin solution was saved for use as input DNA. Immunoprecipitation with the following antibodies was performed: anti-acetyl-Histone H4, anti-acetyl-Histone H3, anti-dimethyl-Histone H3 Lys4, and anti-dimethyl-Histone H3 Lys9 (Upstate USA Inc.). The DNA was extracted using phenol-chloroform, precipitated with ethanol, and dissolved in water. Immunoprecipitations were analyzed by nested PCR using GeneAmp PCR System 9700 (Applied Biosystems). The cycle number and the amount of template were optimized to ensure that results were within the linear range of amplification. The PCR products were size fractionated through 1.0% agarose/ethidium bromide gels.

Quantification of histone acetylation and methylation at *Hoxa7* and *Hoxa9* promoters in $Mll^{PTD/WT}$, $Mll^{WT/-}$ (generously provided by the late S. Korsmeyer), and $Mll^{WT/WT}$ DNA extracted from spleen and BM cells was undertaken using real-time quantitative PCR with SYBR green incorporation (Applied Biosystems). Primers were designed and optimized to amplify genomic sequences in the *Hoxa7* and *Hoxa9* promoters (Supplemental Tables 1 and 2). Each reaction used 2 μl of DNA template and 12.5 μl SYBR Green PCR Master Mix (Applied Biosystems) and was normalized to input DNA. The specificity of PCR products was analyzed by addition of a melting curve cycle, which consisted of 1 cycle each of 60°C for 15 seconds, 95°C for 20 seconds, and 60°C for 15 seconds, followed by analysis on Dissociation Curve Analysis software, version 1.0 (Applied Biosystems).

*Comparative real-time RT-PCR*. Total RNA was extracted from mouse BM, spleen, and peripheral blood samples and cDNA prepared as previously described (41). Primer and probe sets to detect murine *Hoxa7*, *Hoxa9*, and *Hoxa10* transcripts were designed using Primer Express (Applied Biosystems). Real-time RT-PCR efficiency was optimized for each primer/probe set using established guidelines (User Bulletin, Applied Biosystems; http://www.appliedbiosystems.com/support/apptech/). Comparative real-time RT-PCR was performed following the manufacturer's suggested procedures and using the ABI Prism 7700 Sequence Detection System (Applied Biosystems). To normalize for RNA content, the r18s primer/probe set was included in multiplex reactions. Data were analyzed using SDS version 1.7a software (Applied Biosystems) and reported as $2^{-\Delta\Delta Ct}$, which represents the fold differences when normalized to an internal control (r18s) and then compared with $Mll^{WT/WT}$ sibling control samples analyzed on the same 96-well plate. For cell-sorting real-time RT-PCR experiments, whole BM cells were harvested and stained with antibodies to Ter119, CD71, Gr-1, CD11b, B220, and CD3. A minimum of $1 \times 10^5$ cells positive for each lineage marker was isolated using a FACSVantage (BD). Equivalent numbers of cells positive for each marker from $Mll^{WT/WT}$ and $Mll^{PTD/WT}$ were used to quantify *HoxA* gene expression. Real-time RT-PCR was then performed as described above. We used our previously published methodology to quantify absolute levels of *Mll* PTD and *Mll* WT transcripts present in BM, spleen, and blood of $Mll^{PTD/WT}$ mice by real-time RT-PCR (13). Further information on primers and probes is provided in Supplemental Methods.

*Flow cytometric analysis for lineage and subset determination, proliferation, and apoptosis*. Cell lineages and hematopoietic subsets within the BM, spleen, and peripheral blood were assessed using lineage-specific antibodies as previously described (15, 41). Immunofluorescent analysis of antigen expression was performed using a FACSCalibur (BD) and CellQuest software (version 3.3; BD). For quantitative assessment of cellular proliferation, BrdU incorporation was measured according to the manufacturer's protocol (BD Biosciences — Pharmingen). To assess differences in apoptosis, annexin V and PI staining were used and performed according to manufacturer's protocol (BD Biosciences — Pharmingen).

*Whole mount in situ*. Whole mount in situ was performed on E12.5 embryos as previously described (1), using digoxygenin-labeled riboprobes generated according to manufacturer's protocols (Roche Diagnostics). Primer pairs used to generate both sense and anti-sense probes first standardized on WT embryos can be obtained in Supplemental Tables 1 and 2.

*Skeletal analysis*. Intact skeletons were prepared using sex-matched $Mll^{PTD/WT}$ and $Mll^{WT/WT}$ mice 20 weeks of age using previously described methods (42). The microCT images were performed as follows: the sacral vertebrae specimens were mounted in 50-ml plastic test tubes filled with glycerol and imaged at 32 kV, 1 mA, and 1-second exposure with image intensifier operating in 7-inch mode. The spatial resolution of the images is 60 μm.

*Statistics*. A Wilcoxon's signed-rank test was used to compare differences in CFU growth between the $Mll^{WT/WT}$ and $Mll^{PTD/WT}$ splenocytes. The *Hoxa7*, *Hoxa9*, and *Hoxa10* expression levels for each tissue were compared between $Mll^{WT/WT}$ and $Mll^{PTD/WT}$ mice using a 2-sample 2-tailed Student's $t$ test.

## Acknowledgments

This work was funded in part by the Lady Tata Memorial Trust Award (to A.M. Dorrance) and National Cancer Institute grant funding (R01 CA89341 to M.A. Caligiuri, K01 CA96887 to S.P. Whitman, and K08 CA089317 to L.J. Rush). The microCT images were provided by Kim Powell at the Cleveland Clinic Musculoskeletal Imaging Core, funded in part by a National Institute of Arthritis and Musculoskeletal and Skin Diseases (NIAMS) Core Center grant (P30 AR050953-01). We thank Jay Hess for kindly providing the Meis1 primer/probe set for quantification of Meis1 transcript, Terry Rabbitts and John Kersey for providing the $Mll^{af9/WT}$ mice, the late Stanley Korsmeyer for providing the $Mll^{WT/-}$ mice, and the staff of the Transgenic Animal, DNA, and Mouse Phenotyping Shared Resources at The Ohio State University Comprehensive Cancer Center for their assistance.

Received for publication May 3, 2005, and accepted in revised form July 25, 2006.

Address correspondence to: Michael A. Caligiuri, The Ohio State University, Comprehensive Cancer Center, 320 West 10th Avenue, Columbus, Ohio 43220, USA. Phone: (614) 293-7521; Fax: (614) 293-7522; E-mail: michael.caligiuri@osumc.edu.

1. Yu, B.D., Hess, J.L., Horning, S.E., Brown, G.A., and Korsmeyer, S.J. 1995. Altered Hox expression and segmental identity in Mll-mutant mice. *Nature.* **378**:505–508.
2. Zeleznik-Le, N.J., Harden, A.M., and Rowley, J.D. 1994. 11q23 translocations split the "AT hook" cruciform DNA binding region and the transcriptional repression domain from the activation domain of the mixed-lineage leukemia (MLL) gene. *Proc. Natl. Acad. Sci. U. S. A.* **91**:10610–10614.
3. Caligiuri, M.A., et al. 1994. Molecular rearrangement of the ALL-1 gene in acute myeloid leukemia without cytogenetic evidence of 11q23 chromosomal translocations. *Cancer Res.* **54**:370–373.
4. Caligiuri, M., et al. 1998. Rearrangement of *ALL1* (*MLL*) in acute myeloid leukemia with normal cytogenetics. *Cancer Res.* **58**:55–59.
5. Dohner, K., et al. 2002. Prognostic significance of partial tandem duplications of the MLL gene in adult patients 16 to 60 years old with acute myeloid leukemia and normal cytogenetics: a study of the Acute Myeloid Leukemia Study Group Ulm. *J. Clin. Oncol.* **20**:3254–3261.
6. Golub, T.R., et al. 1999. Molecular classification of cancer: class discovery and class prediction by gene expression monitoring. *Science.* **286**:531–537.
7. Nakamura, T., et al. 2002. ALL-1 is a histone methyltransferase that assembles a supercomplex of proteins involved in transcriptional regulation. *Mol. Cell.* **10**:1119–1128.
8. Milne, T.A., et al. 2002. MLL targets SET domain methyltransferase activity to Hox gene promoters. *Mol. Cell.* **10**:1107–1117.
9. Milne, T.A., Martin, M.E., Brock, H.W., Slany, R.K., and Hess, J.L. 2005. Leukemogenic MLL fusion proteins bind across a broad region of the Hox a9 locus, promoting transcription and multiple histone modifications. *Cancer Res.* **65**:11367–11374.
10. Kumar, A.R., et al. 2004. Hoxa9 influences the phenotype but not the incidence of Mll-AF9 fusion gene leukemia. *Blood.* **103**:1823–1828.
11. Dobson, C.L., et al. 1999. The mll-AF9 gene fusion in mice controls myeloproliferation and specifies acute myeloid leukaemogenesis. *EMBO J.* **18**:3564–3574.
12. Hsieh, J.J., Cheng, E.H., and Korsmeyer, S.J. 2003. Taspase1: a threonine aspartase required for cleavage of MLL and proper HOX gene expression. *Cell.* **115**:293–303.
13. Whitman, S.P., et al. 2005. The MLL partial tandem duplication: evidence for recessive gain-of-function in acute myeloid leukemia identifies a novel patient subgroup for molecular-targeted therapy. *Blood.* **106**:345–352.
14. Caligiuri, M.A., et al. 1997. The partial tandem duplication of ALL1 in acute myeloid leukemia with normal cytogenetics or trisomy 11 is restricted to 1 chromosome. *Proc. Natl. Acad. Sci. U. S. A.* **94**:3899–3902.
15. Na Nakorn, T., Traver, D., Weissman, I.L., and Akashi, K. 2002. Myeloerythroid-restricted progenitors are sufficient to confer radioprotection and provide the majority of day 8 CFU-S. *J. Clin. Invest.* **109**:1579–1585. doi:10.1172/JCI200215272.
16. Nakamura, T., Largaespada, D.A., Shaughnessy, J.D., Jr., Jenkins, N.A., and Copeland, N.G. 1996. Cooperative activation of Hoxa and Pbx1-related genes in murine myeloid leukaemias. *Nat. Genet.* **12**:149–153.
17. Moskow, J.J., Bullrich, F., Huebner, K., Daar, I.O., and Buchberg, A.M. 1995. Meis1, a PBX1-related homeobox gene involved in myeloid leukemia in BXH-2 mice. *Mol. Cell. Biol.* **15**:5434–5443.
18. Kroon, E., et al. 1998. Hoxa9 transforms primary bone marrow cells through specific collaboration with Meis1a but not Pbx1b. *EMBO J.* **17**:3714–3725.
19. Duboule, D., and Dolle, P. 1989. The structural and functional organization of the murine HOX gene family resembles that of Drosophila homeotic genes. *EMBO J.* **8**:1497–1505.
20. Kessel, M., Balling, R., and Gruss, P. 1990. Variations of cervical vertebrae after expression of a Hox-1.1 transgene in mice. *Cell.* **61**:301–308.
21. Morgan, B.A., Izpisua-Belmonte, J.C., Duboule, D., and Tabin, C.J. 1992. Targeted misexpression of Hox-4.6 in the avian limb bud causes apparent homeotic transformations. *Nature.* **358**:236–239.
22. Lufkin, T., et al. 1992. Homeotic transformation of the occipital bones of the skull by ectopic expression of a homeobox gene. *Nature.* **359**:835–841.
23. Fromental-Ramain, C., et al. 1996. Specific and redundant functions of the paralogous Hoxa-9 and Hoxd-9 genes in forelimb and axial skeleton patterning. *Development.* **122**:461–472.
24. Drabkin, H.A., et al. 2002. Quantitative HOX expression in chromosomally defined subsets of acute myelogenous leukemia. *Leukemia.* **16**:186–195.
25. Rozovskaia, T., et al. 2001. Upregulation of Meis1 and HoxA9 in acute lymphocytic leukemias with the t(4:11) abnormality. *Oncogene.* **20**:874–878.
26. Fujino, T., et al. 2001. Inhibition of myeloid differentiation by Hoxa9, Hoxb8, and Meis homeobox genes. *Exp. Hematol.* **29**:856–863.
27. Buske, C., and Humphries, R.K. 2000. Homeobox genes in leukemogenesis. *Int. J. Hematol.* **71**:301–308.
28. Buske, C., et al. 2001. Overexpression of HOXA10 perturbs human lymphomyelopoiesis in vitro and in vivo. *Blood.* **97**:2286–2292.
29. Kawagoe, H., Humphries, R.K., Blair, A., Sutherland, H.J., and Hogge, D.E. 1999. Expression of HOX genes, HOX cofactors, and MLL in phenotypically and functionally defined subpopulations of leukemic and normal human hematopoietic cells. *Leukemia.* **13**:687–698.
30. Armstrong, S.A., et al. 2002. MLL translocations specify a distinct gene expression profile that distinguishes a unique leukemia. *Nat. Genet.* **30**:41–47.
31. Jenuwein, T., and Allis, C.D. 2001. Translating the histone code. *Science.* **293**:1074–1080.
32. Zhang, Y., and Reinberg, D. 2001. Transcription regulation by histone methylation: interplay between different covalent modifications of the core histone tails. *Genes Dev.* **15**:2343–2360.
33. Lachner, M., and Jenuwein, T. 2002. The many faces of histone lysine methylation. *Curr. Opin. Cell Biol.* **14**:286–298.
34. Ernst, P., Wang, J., Huang, M., Goodman, R.H., and Korsmeyer, S.J. 2001. MLL and CREB bind cooperatively to the nuclear coactivator CREB-binding protein. *Mol. Cell. Biol.* **21**:2249–2258.
35. Petruk, S., et al. 2001. Trithorax and dCBP acting in a complex to maintain expression of a homeotic gene. *Science.* **294**:1331–1334.
36. Milne, T.A., et al. 2005. MLL associates specifically with a subset of transcriptionally active target genes. *Proc. Natl. Acad. Sci. U. S. A.* **102**:14765–14770.
37. Martin, M.E., et al. 2003. Dimerization of MLL fusion proteins immortalizes hematopoietic cells. *Cancer Cell.* **4**:197–207.
38. Steudel, C., et al. 2003. Comparative analysis of MLL partial tandem duplication and FLT3 internal tandem duplication mutations in 956 adult patients with acute myeloid leukemia. *Genes Chromosomes Cancer.* **37**:237–251.
39. Quentmeier, H., Reinhardt, J., Zaborski, M., and Drexler, H.G. 2003. MLL partial tandem duplications in acute leukemia cell lines. *Leukemia.* **17**:980–981.
40. Caligiuri, M.A., et al. 1996. Partial tandem duplication of ALL1 as a recurrent molecular defect in acute myeloid leukemia with trisomy 11. *Cancer Res.* **56**:1418–1425.
41. Fehniger, T.A., et al. 2001. Fatal leukemia in interleukin 15 transgenic mice follows early expansions in natural killer and memory phenotype CD8(+) T cells. *J. Exp. Med.* **193**:219–232.
42. McLeod, M.J. 1980. Differential staining of cartilage and bone in whole mouse fetuses by alcian blue and alizarin red S. *Teratology.* **22**:299–301.